

https://dspace.org/

Study of nonlinear MHD tribological squeeze film at generalized magnetic reynolds numbers using DTM.

Rashidi, M.M.; Freidoonimehr, N.; Momoniat, E.; Rostami, B.

2015-08-12
Public Library of Science
http://hdl.handle.net/10539/20431
Rashidi, M.M. et al. 2015. Study of nonlinear MHD tribological squeeze film at generalized magnetic reynolds numbers using DTM. PLoS ONE 10(8), pp.1-21

Downloaded from a DSpace repository. https://dspace.org/

PLOS ONE

RESEARCH ARTICLE

Study of Nonlinear MHD Tribological Squeeze Film at Generalized Magnetic Reynolds Numbers Using DTM

Mohammad Mehdi Rashidi[1,2]*, Navid Freidoonimehr[3], Ebrahim Momoniat[4], Behnam Rostami[3]

1 Mechanical Engineering Department, Engineering Faculty of Bu-Ali Sina University, Hamedan, Iran, **2** University of Michigan-Shanghai Jiao Tong University Joint Institute, Shanghai Jiao Tong University, Shanghai, Peoples Republic of China, **3** Young Researchers & Elite Club, Hamedan Branch, Islamic Azad University, Hamedan, Iran, **4** DST/NRF Centre of Excellence in the Mathematical and Statistical Sciences, School of Computer Science and Applied Mathematics, University of the Witwatersrand, Johannesburg, Private Bag 3, Wits 2050, South Africa

* mm_rashidi@sjtu.edu.cn

CrossMark
click for updates

OPEN ACCESS

Citation: Rashidi MM, Freidoonimehr N, Momoniat E, Rostami B (2015) Study of Nonlinear MHD Tribological Squeeze Film at Generalized Magnetic Reynolds Numbers Using DTM. PLoS ONE 10(8): e0135004. doi:10.1371/journal.pone.0135004

Editor: Saeed Islam, Abdul Wali Khan university Mardan Pakistan, PAKISTAN

Received: March 2, 2015

Accepted: July 16, 2015

Published: August 12, 2015

Copyright: © 2015 Rashidi et al. This is an open access article distributed under the terms of the Creative Commons Attribution License, which permits unrestricted use, distribution, and reproduction in any medium, provided the original author and source are credited.

Data Availability Statement: All relevant data are within the paper and its Supporting Information files.

Funding: EM acknowledges support from the National Research foundation of South Africa. The funders had no role in study design, data collection and analysis, decision to publish, or preparation of the manuscript.

Competing Interests: The authors have declared that no competing interests exist.

Abstract

In the current article, a combination of the differential transform method (DTM) and Padé approximation method are implemented to solve a system of nonlinear differential equations modelling the flow of a Newtonian magnetic lubricant squeeze film with magnetic induction effects incorporated. Solutions for the transformed radial and tangential momentum as well as solutions for the radial and tangential induced magnetic field conservation equations are determined. The DTM-Padé combined method is observed to demonstrate excellent convergence, stability and versatility in simulating the magnetic squeeze film problem. The effects of involved parameters, i.e. squeeze Reynolds number (N_1), dimensionless axial magnetic force strength parameter (N_2), dimensionless tangential magnetic force strength parameter (N_3), and magnetic Reynolds number (Re_m) are illustrated graphically and discussed in detail. Applications of the study include automotive magneto-rheological shock absorbers, novel aircraft landing gear systems and biological prosthetics.

Introduction

Understanding magneto-hydrodynamics (MHD) is strongly related to the comprehension of physical effects which take place in MHD. When a conductor moves into a magnetic field, electric current is induced in the conductor and creates its own magnetic field (Lenz's law). Since the induced magnetic field tends to eliminate the original and external supported field, the magnetic field lines will be excluded from the conductor. Conversely, when the magnetic field influences the conductor to move it out of the field, the induced field amplifies the applied field. The net result of this process is that the lines of force appear to be dragged accompanied by the conductor. In this paper the conductor is the fluid with complex motions. To understand the second key effect which is dynamical we should know that when currents are induced by a motion of a conducting fluid through a magnetic field, a Lorentz force acts on the fluid and modifies its motion. In MHD, the motion modifies the field and vice versa. This makes the theory highly non-linear [1, 2].

In recent decades, researchers have performed several studies in the fields of the MHD applications'. Khan *et al.* [3] investigated the effects of an arbitrary wall shear stress on unsteady MHD flow of a Newtonian fluid with conjugate effects of heat and mass transfer using the Laplace transform technique. Hussanan *et al.* [4] analysed the unsteady boundary layer MHD free convection flow past an oscillating vertical plate embedded in a porous medium with constant mass diffusion and Newtonian heating condition using the Laplace transform technique. Samiulhaq *et al.* [5] studied the magnetic field influence on unsteady free convection flow of a second grade fluid near an infinite vertical flat plate with ramped wall temperature embedded in a porous medium. In another study, Khan *et al.* [6] displayed the effects of an arbitrary wall shear stress on unsteady MHD flow of a Newtonian fluid with conjugate effects of heat and mass transfer. Further, Khalid *et al.* [7] illustrated the unsteady MHD free flow of a Casson fluid past an oscillating vertical plate with constant wall temperature.

Magneto-hydrodynamic lubrication is a type of "smart tribology" which has found increasing applications in diverse branches of engineering in recent years. These include seismic magneto-rheological (MR) shock dampers [8], magnetic-repulsion enhanced hydrostatic bearings for offshore wave energy conversion devices [9], and biomedical systems [10, 11]. MHD lubricants respond to the application of magnetic fields and have been presented to enhance load-carrying capacities, reduce wear and achieve more uniform pressure distributions. A tremendous variety of such lubricants has been developed including ferrofluids, magnetic particle-based suspensions, electrically-conducting biopolymers and yield stress magnetic fluids. In parallel with practical and manufacturing developments, there has been a rich contribution from engineering scientists engaged in mathematical and experimental simulations of the behaviour of such fluids in many complex tribological configurations.

Chandra *et al.* [12] studied electromagnetic lubrication in various journal bearings with cavitation boundary conditions and for regimes where the magnetization vector is oblique to the magnetic field vector, showing that better contact performance is achieved compared with non-magnetic lubricants. Song *et al.* [13] analysed wear and friction characteristics of a magneto-rheological fluid under different magnetic fields, by employing a pin-on-disc tribometer, and showed that MR fluid exhibits improved lubrication characteristics. They also observed that the key wear mechanism for steel and brass specimens was abrasive wear by asperities and MR particles on the worn surfaces, whereas a mixed wear mechanism that included adhesive wear and abrasive wear was observed for the aluminium specimen studied. Durán *et al.* [14] presented a novel formulation of a stable magnetic fluid to show that the yield stress is elevated by several orders of magnitude when the magnetic field strength reaches several hundred microTesla, and furthermore observed that excellent damping of forced oscillations is achievable in automotive magneto-fluid bearings. Huang *et al.* [15] investigated ferrofluid magnetic tribology for lubricants comprising stable colloidal systems consisting of single-domain magnetic particles with a diameter of approximately 10 nm coated with surfactants and dispersed in a carrier liquid. By applying an external magnetic field, they demonstrated that ferrofluid lubricants may be orientated and positioned at optimized locations. They additionally showed that the load capacity of a Fe_3O_4-based ferrofluid lubricant film may be significantly boosted with appropriate magnetic field and that these liquids achieve a good friction-reduction performance in the presence of an external magnetic field compared with the carrier liquid with markedly enhanced lifetimes. Stolarsky and Makida [16] conducted experiments on the effect of permanent magnetic fields on the wear of lubricated sliding contact operating at short stroke and high frequency, observing that horizontal magnetic field strongly influences contact performance. They also noted that magnetic field increases the abrasive action by wear particles and allows reduction in wear of the plate specimen. An especially significant regime in magneto-hydrodynamic tribology is the squeeze film. This has attracted considerable attention as it

can be simulated using classical methods of elasto-hydrodynamics (EHD). Anwar and Rodkiewicz [17] examined computationally the MHD squeeze lubrication of a slider bearing system, including inertia effects and considering low Hartmann numbers. They found that inertial terms have a reduced influence with greater Hartmann number and that a non-uniform magnetic field achieves noticeably greater load capacity than uniform magnetic fields.

In recent years many sophisticated numerical and so-called semi-numerical/analytical procedures have been implemented to solve boundary value problems arising in magnetic tribology and also nonlinear squeeze film flows. Kargulewicz *et al.* [18] developed a discrete element algorithm to optimize aircraft ejector seat applications. Zueco and Bég [19] applied the electrothermal network simulation code to study magneto-elastic hydrodynamic lubrication between rotating disks at generalized magnetic Reynolds numbers, as a model of conceptual spacecraft landing gear systems for Mars NASA missions. Zhu and Ingber [20] utilized a traction-modified boundary element method (BEM) to study Newtonian squeeze films between spherical bodies in locomotive gear systems. Gertzos *et al.* [21] studied the performance characteristics of a hydrodynamic journal bearing lubricated with either magneto-rheological Bingham or electro-rheological Bingham fluids using the commercial CFD software, FLUENT software with a "dynamic meshing" technique. Bég *et al.* [22] analyzed the magneto-hydrodynamic squeezing flow of a microstructural fluid in a porous media biological bearing with the Liao homotopy analysis method (HAM), observing that micro-rotation of lubricant micro-elements is strongly influenced by Hartmann number and medium permeability, and that response time is also enhanced with magnetic field. Moghani *et al.* [23] used a hybrid fluid-solid meshing procedure in the ADINA commercial finite element code to study squeezing lubrication of soft biomaterials. From the above squeezing hydrodynamics studies which have considered magnetic fields, with the exception of Zueco and Bég [19] have generally neglected magnetic induction effects. When magnetic Reynolds number is sizeable, an induced magnetic field is also generated in the flow and a separate magnetic field conservation equation is required. Several researchers have studied magnetic induction effects. Elshekh and Elhady [24] investigated magnetic squeeze film flow between co-rotating disks with induced magnetic field effects, computing the response of radial and azimuthal magnetic fields to squeezing rates and relative disk rotation, although only for a single value of Batchelor number. Gul *et al.* [25] demonstrated the problem of thin film layer flowing on a vertical oscillating belt via two analytical techniques namely Adomian Decomposition Method (ADM) and Optimal Homotopy Asymptotic Method (OHAM). In another study, Gul *et al.* [26] performed an analysis to study the unsteady thin film flow of a second grade fluid over a vertical oscillating belt.

Nonlinear differential equations are employed to describe some of physical systems. Concurrent with the development of computers, rising use of analytical methods can be observed in comparison with numerical methods. Despite all the benefits, there are a lot of cons for the numerical methods such as the inability to apply infinite boundary condition, etc. There are a lot of analytical methods such as DTM [27, 28], HAM [29, 30], HPM [31], and ADM [32] applied to solve nonlinear equations. The main advantage of these methods applied to nonlinear differential equations is that no linearization or discretization needs to take place [33]. In the present article we employ DTM-Padé method to analyse two nonlinear magneto-hydrodynamic squeeze film boundary value problems. The present DTM-Padé code is also benchmarked with the numerical method based on shooting technique, illustrating excellent correlation. Excellent convergence and stability characteristics are also observed for the DTM-Padé code. The present simulations find applications in novel aircraft landing gear systems exploiting smart magnetic fluids.

The paper is divided up as follows: in section 2 we derive the mathematical model we will be investigating in this paper. In section 3 we implement the DTM-Padé method to solve the

resulting system of nonlinear differential equations. Results are discussed in section 4. Concluding remarks are presented in section 5.

Mathematical Model

In this problem, we assume the axisymmetric flow in a polar coordinate system (r, θ, z) of a thin Newtonian, hydro-magnetic lubricant fluid squeeze film between two disks placed parallel to each other and each rotating at constant velocity in its own plane. The components of the flow velocity (u, v, w) are in the directions of increasing (r, θ, z), respectively. The disks are separated by a distance $D(1 - \alpha t)^{1/2}$ at time t, where D is a representative length equivalent to the disk separation at $t = 0$ and t denotes time. The coordinate system and the physical regime of the problem are shown in Fig 1.

The upper disk can moves downwards at velocity $d(d(t))/dt$ (where $d(t)$ is separation of the disks at time t), towards the constrained lower disk. In the other words, the lower disk is prohibited from moving in the axial direction (along the z-axis). The applied magnetic field (H) has two components; include an azimuthal (tangential) component (H_θ) and an axial component (H_z) which affect the upper disk. These parameters are defined as $H_\theta = r\,N_0/(\mu_2(1 - \alpha t))$ and $H_z = -\alpha\,M_0/(\mu_1(1 - \alpha t)^{1/2})$, where M_0 and N_0 are the magnetic field quantities introduced to render H_θ and H_z, dimensionless, μ_2 and μ_1 are the magnetic permeability's of the squeeze film and the medium external to the disks, respectively. For liquid metals $\mu_2 = \mu_0$, where μ_0 is the permeability of free space. Following the experimental study, H_θ and H_z are assumed to be zero on the lower disk [24]. This applied magnetic field (H) generates an induced magnetic field B with components (B_r, B_θ, B_z) in the squeeze film, between the disks. By neglecting the convective acceleration components in the Navier–Stokes equations and considering the above assumptions, the governing equations of the hydro-magnetic squeeze film regime for the momentum and magnetic field equations in a (r, θ, z) coordinate system are [24, 34, 35]:

$$\frac{\partial u}{\partial t} = \nu\frac{\partial^2 u}{\partial z^2} - \frac{1}{\rho\,\mu_2}\left(2\,r\,M\frac{\partial^2 M}{\partial z^2}\right), \tag{1}$$

$$\frac{\partial v}{\partial t} = \nu\frac{\partial^2 v}{\partial z^2} - \frac{1}{\rho\,\mu_2}\left(2\,r\,M\frac{\partial^2 N}{\partial z^2}\right), \tag{2}$$

$$0 = \nu\frac{\partial^2 w}{\partial z^2} - \frac{1}{\rho\,\mu_2}\left(r^2 N\frac{\partial N}{\partial z} - r^2\frac{\partial^3 N}{\partial z^3}\right), \tag{3}$$

$$\frac{\partial B_r}{\partial t} = -r\frac{\partial^3 M}{\partial z^3} + \frac{1}{\sigma\,\mu_2}\left(\frac{\partial^2 B_r}{\partial z^2}\right), \tag{4}$$

$$\frac{\partial B_\theta}{\partial t} = -r\frac{\partial^2 N}{\partial z^2} + \frac{1}{\sigma\,\mu_2}\left(\frac{\partial^2 B_\theta}{\partial z^2}\right), \tag{5}$$

$$\frac{\partial B_z}{\partial t} = \frac{1}{\sigma\,\mu_2}\left(\frac{\partial^2 B_z}{\partial z^2}\right), \tag{6}$$

where ν is the kinematic fluid viscosity, ρ is fluid density, μ_2 is magnetic permeability of the medium between the two disks (squeeze film regime) and σ is the electrical conductivity of fluid (squeeze film).

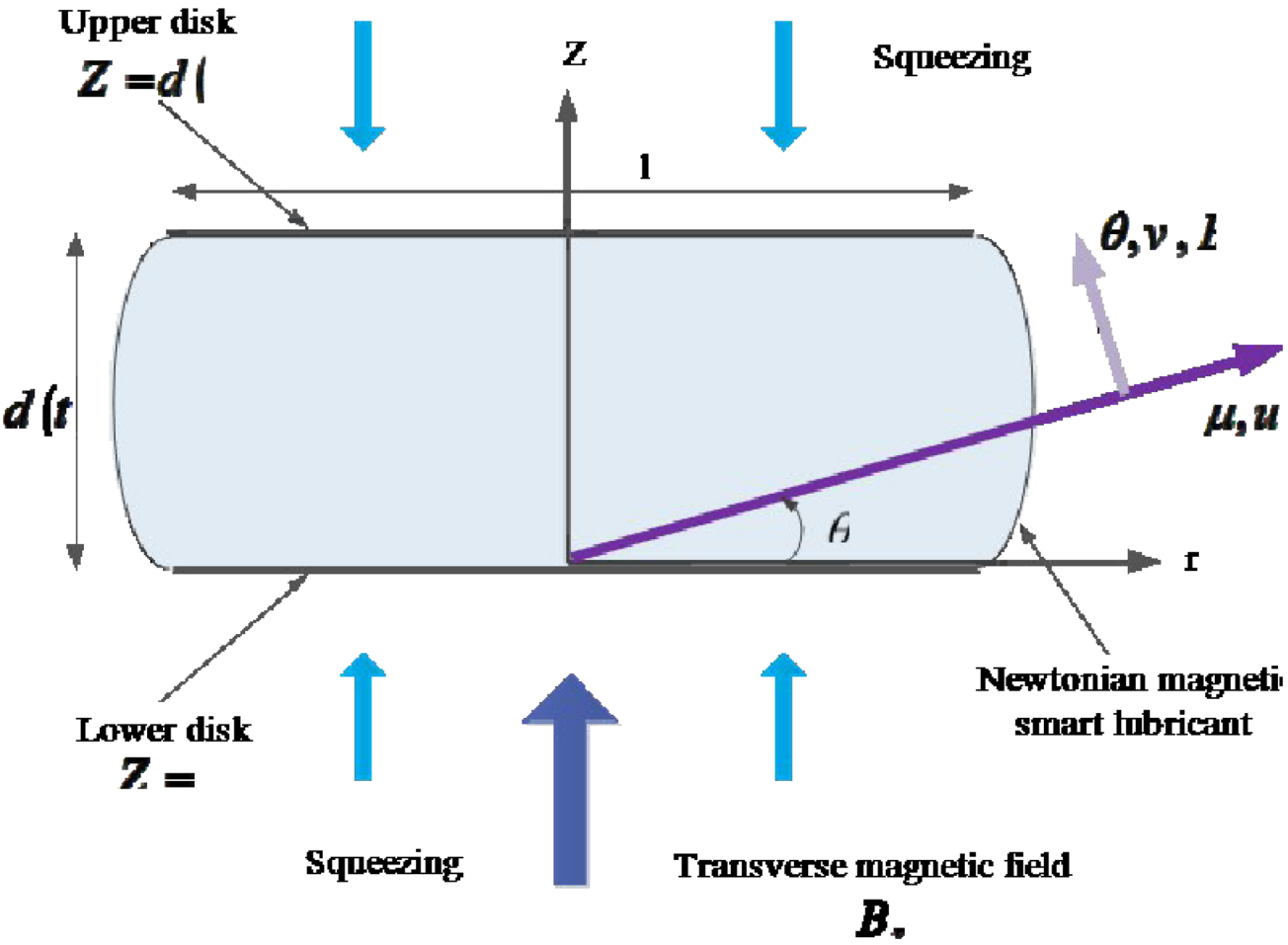

Fig 1. Hydromagnetic rotating squeeze film lubrication with magnetic induction.

doi:10.1371/journal.pone.0135004.g001

It should be noticed that the Eqs (4)–(6) are the components of magnetic field equation $\frac{\partial \mathbf{B}}{\partial t} = \nabla \times (\nabla \times \mathbf{B}) + \frac{1}{\sigma \mu_2} \nabla^2 \mathbf{B}$ in the directions of polar coordinate system, where $\mathbf{B} = \mu_2 \mathbf{H}$ [24, 36]. The governing equations can be reduced from a system of partial differential equations (PDEs) to dimensionless, coupled and nonlinear ordinary differential equations (ODEs) by introducing the following transformations:

$$\eta = \frac{z}{d(t)} \qquad d(t) = D(1-\alpha\xi)^{1/2}$$

$$u = r\frac{\partial F(z,t)}{\partial z} = \frac{\alpha r \frac{df}{d\eta}}{2(1-\alpha\xi)} \qquad v = rG(z,t) = \frac{r\Omega_1 g(\eta)}{(1-\alpha\xi)}$$

$$w = -2F(z,t) = -\frac{\alpha D f(\eta)}{(1-\alpha\xi)^{1/2}} \qquad B_r = r\frac{\partial M(z,t)}{\partial z} = \frac{\alpha r M_0 \frac{dm(\eta)}{d\eta}}{2D(1-\alpha\xi)} \tag{7}$$

$$B_\theta = rN(z,t) = \frac{rN_0 n(\eta)}{(1-\alpha\xi)} \qquad B_z = -2M(z,t) = -\frac{\alpha M_0 m(\eta)}{(1-\alpha\xi)^{1/2}}$$

Substituting Eq 7 in Eqs (1)–(6), we obtain the following dimensionless system of highly nonlinear and coupled ordinary differential equations in terms of a single independent space variable (η):

$$\frac{d^4f}{d\eta^4} = N_1\left(3\frac{d^2f}{d\eta^2} + (\eta - 2f)\frac{d^3f}{d\eta^3} - 2N_2{}^2 m\frac{d^2m}{d\eta^2}\right), \tag{8}$$

$$\frac{d^2g}{d\eta^2} = N_1\left(2g + \eta\frac{dg}{d\eta} + 2g\frac{df}{d\eta} - 2f\frac{dg}{d\eta} + 2N_2N_3\left(m\frac{dn}{d\eta} - n\frac{dm}{d\eta}\right)\right), \tag{9}$$

$$\frac{d^2m}{d\eta^2} = Re_m\left(m + \eta\frac{dm}{d\eta} - 2f\frac{dm}{d\eta} + 2m\frac{df}{d\eta}\right), \tag{10}$$

$$\frac{d^2n}{d\eta^2} = Re_m\left(2n + \eta\frac{dn}{d\eta} - 2f\frac{dn}{d\eta} + 2\left(\frac{N_2}{N_3}\right)m\frac{dg}{d\eta}\right), \tag{11}$$

where η is dimensionless z-coordinate, f is dimensionless axial velocity, g is dimensionless tangential velocity, m is dimensionless axial induced magnetic field component, n is dimensionless tangential induced magnetic field component, $N_1(=\alpha D^2/2\nu)$ is squeeze Reynolds number (based on the speed of approach of the two disks), represents the ratio between the normal (axial) velocity of the upper disk and kinematic viscosity, $N_2(=M_0/D\sqrt{\mu_2\rho})$ is dimensionless parameter based on the magnetic force in the axial direction, $N_3(=N_0/\Omega_1\sqrt{\mu_2\rho})$ is dimensionless parameter based on magnetic force strength in the azimuthal (tangential) direction, $Re_m(=N_1Bt)$ is magnetic Reynolds number and $Bt(=\sigma\mu_2\nu)$ is the Batchelor number. As it is obvious from Eqs (8)–(11) the variation in the magnetic Reynolds number can be varied by keeping N_1 invariant and altering Batchelor number (Bt) or vice versa. According to the Hughes and Elco [37], it is considered that both disks are ideal (perfect) conductors. Electrical forces are much smaller than the magnetic forces and consequently are ignored in the present problem. The boundary conditions for the magnetic induction **B** follow from the fact that the normal component of **B** and the tangential component of **H** are continuous through the two disks. The transformed boundary conditions become:

$$\begin{aligned} &f(0) = \frac{df(0)}{d\eta} = 0,\ \ g(0) = 1,\ \ m(0) = n(0) = 0, && \text{at} \quad \eta = 0\,(\textit{Lower disk}),\\ &f(1) = 0.5,\ \ \frac{df(1)}{d\eta} = 0,\ \ g(1) = 0,\ \ m(1) = n(1) = 1, && \text{at} \quad \eta = 1\,(\textit{Upper disk}), \end{aligned} \tag{12}$$

In tribological applications, we can further define the dimensionless frictional moment's i.e. non-dimensional torques exerted on the upper and lower disks. The torque at the upper disk is

$$T_{Upper\ disk} = 2\pi\mu\int_0^a\left(\frac{\partial v}{\partial z}\right)_{z=d}dr, \tag{13}$$

where μ m denotes the Newtonian dynamic viscosity. Using (7) and (13), we obtain:

$$\bar{T}_{Upper\ disk} = \frac{2D(1-\alpha\xi)^{3/2}}{\pi\mu\Omega_1 a^4}T_{Upper\ disk} = \frac{dg(1)}{d\eta}, \tag{14}$$

where $\bar{T}_{Upper\ disk}$ is the dimensionless torque exerted by the fluid on the upper disk and $dg(1)/d\eta$ is the azimuthal (tangential) velocity gradient at the upper disk ($\eta = 1$). Similarly for the lower

disk, the dimensionless torque is simply given by the same calculation evaluated at $\eta = 0$, as

$$\bar{T}_{Lower\ disk} = \frac{dg(0)}{d\eta}, \tag{15}$$

where $dg(0)/d\eta$ is the tangential (azimuthal) velocity gradient at the lower disk ($\eta = 0$).

The Differential Transform Method

DTM is employed to obtain semi- analytical/numerical solutions to the well-posed two-point boundary value problem defined by Eqs (8)–(11) and conditions (12). DTM is an extremely strong technique in finding solutions to magneto-hydrodynamic and complex material flow problems. It has also been used very effectively in conjunction with Padé approximants. To provide a summary of the method, the transformation of the kth derivative of a function in one variable is considered which is defined as:

$$F(k) = \frac{1}{k!}\left[\frac{d^k f(\eta)}{d\eta^k}\right]_{\eta=\eta_0}, \tag{16}$$

where $f(\eta)$ is the original function and $F(k)$ is transformed function. The differential inverse transformation of $F(k)$ is:

$$f(\eta) = \sum_{k=0}^{\infty} F(k)(\eta - \eta_0)^k, \tag{17}$$

The concept of the differential transform is derived from a Taylor series expansion and in actual applications the function $f(\eta)$ is expressed by a finite series as follows:

$$f(\eta) \cong \sum_{k=0}^{m} F(k)(\eta - \eta_0)^k, \tag{18}$$

The value of m is decided by convergence of the series coefficients.

3.1. Padé Approximant

Páde approximants are applied to the problem to increase the convergence of a given series. Suppose that a power series $\sum_{i=0}^{\infty} a_i x^i$ is given, which represents a function $f(x)$, such that:

$$f(x) = \sum_{i=0}^{\infty} a_i x^i, \tag{19}$$

The Páde approximant is a rational fraction and the notation for such a Padé approximant is:

$$[L/M] = \frac{P_L(x)}{Q_M(x)}, \tag{20}$$

where $P_L(x)$ is a polynomial of degree at most L and $Q_M(x)$ is a polynomial of degree at most

M. Therefore:

$$f(x) = a_0 + a_1 x + a_2 x^2 + a_3 x^3 + a_4 x^4 + \cdots, \tag{21}$$

$$P_L(x) = p_0 + p_1 x + p_2 x^2 + p_3 x^3 + \ldots + p_L x^L, \tag{22}$$

$$Q_M(x) = q_0 + q_1 x + q_2 x^2 + q_3 x^3 + \ldots + q_M x^M, \tag{23}$$

where in Eq (20) there are $L + 1$ numerator coefficients and $M + 1$ denominator coefficients. Since the numerator and denominator can be multiplied by a constant and $[L/M]$ left unchanged, the following normalization condition is imposed

$$Q_M(0) = 1, \tag{24}$$

So there are $L + 1$ independent numerator coefficients and M independent denominator coefficients, which make $L + M + 1$ unknown coefficients in all. This number suggests that normally the $[L/M]$ ought to fit the power series Eq (19) through the orders $1, x, x^2, \ldots, x^{L+M}$. Based on conditions given in [38, 39], $[L/M]$ approximation is uniquely determined. In the notation of formal power series:

$$\sum_{i=0}^{\infty} a_i x^i = \frac{p_0 + p_1 x + p_2 x^2 + p_3 x^3 + \ldots + p_L x^L}{q_0 + q_1 x + q_2 x^2 + q_3 x^3 + \ldots + q_M x^M} + O(x^{L+M+1}), \tag{25}$$

By cross-multiplying Eq (25), one obtains:

$$\begin{aligned}(p_0 + p_1 x + p_2 x^2 + p_3 x^3 + \ldots + p_L x^L) \times (a_0 + a_1 x + a_2 x^2 + a_3 x^3 + a_4 x^4 + \ldots) \\ = q_0 + q_1 x + q_2 x^2 + q_3 x^3 + \ldots + q_M x^M + O(x^{L+M+1}),\end{aligned} \tag{26}$$

From Eq (26) the following set of linear equations are obtained

$$\begin{cases} a_0 = p_0, \\ a_1 + a_0 q_1 = p_1, \\ a_2 + a_1 q_1 + a_0 q_2 = p_2, \\ \vdots \\ a_L + a_{L-1} q_1 + \cdots + a_0 q_L = p_L, \end{cases} \tag{27}$$

and

$$\begin{cases} a_{L+1} + a_L q_1 + \cdots + a_{L-M+1} q_M = 0, \\ a_{L+2} + a_{L+1} q_1 + \cdots + a_{L-M+2} q_M = 0, \\ \vdots \\ a_{L+M} + a_{L+M-1} q_1 + \cdots + a_L q_M = 0, \end{cases} \tag{28}$$

where $a_n = 0$ for $n < 0$ and $q_j = 0$ for $j > M$. Eqs (27) and (28) can be solved directly if they are

non-singular

$$[L/M] = \frac{\begin{vmatrix} a_{L-m+1} & a_{L-M+2} & \dots & a_{L+1} \\ \vdots & \vdots & \ddots & \vdots \\ a_L & a_{L+1} & \dots & a_{L+M} \\ \sum_{j=M}^{L} a_{j-M}x^j & \sum_{j=M-1}^{L} a_{j-M+1}x^j & \dots & \sum_{j=0}^{L} a_j x^j \end{vmatrix}}{\begin{vmatrix} a_{L-m+1} & a_{L-m+2} & \dots & a_{L+1} \\ \vdots & \vdots & \ddots & \vdots \\ a_L & a_{L+1} & \dots & a_{L+M} \\ x^M & x^{M-1} & \dots & 1 \end{vmatrix}}, \tag{29}$$

If the lower index on a sum exceeds the upper, the sum is replaced by zero. Alternate forms are:

$$[L/M] = \sum_{j=0}^{L-M} a_j x^j + x^{L-M+1} w_{L/M}^T W_{L/M}^{-1} w_{L/M} = \sum_{j=0}^{L+n} a_j x^j + x^{L+n+1} w_{(L+M)/M}^T W_{L/M}^{-1} w_{(L+n)/M}, \tag{30}$$

For

$$W_{L/M} = \begin{bmatrix} a_{L-M+1} - xa_{L-M+2} & \dots & a_L - xa_{L+1} \\ \vdots & \ddots & \vdots \\ a_L - xa_{L+1} & \dots & a_{L+M+1} - xa_{L+M} \end{bmatrix}, \tag{31}$$

$$w_{L/M} = \begin{bmatrix} a_{L-M+1} \\ a_{L-M+2} \\ \vdots \\ a_L \end{bmatrix}, \tag{32}$$

The construction of $[L/M]$ approximants involves only algebraic operations [38, 39]. Each choice of L, degree of the numerator and M, degree of the denominator, leads to an approximant. How to direct the choice in order to obtain the best approximant is the major difficulty in applying the technique, which necessitates the need for a criterion for the choice depending on the *shape* of the solution. A criterion which has worked well here is the choice of $[L/M]$ approximants such that $L = M$.

3.2. Analytical approximation by means of DTM-Padé

Taking differential transform of Eqs (8)–(11), one can obtain (for more details, see [40–42])

$$(k+1)(k+2)(k+3)(k+4)f(k+4)- N_1\left(\begin{array}{c} 3(k+1)(k+2)f(k+2)+ \\ \sum_{r=0}^{k}\left(\begin{array}{c}(k-r+1)(k-r+2)(k-r+3)\delta(r)f(k-r+3)- \\ 2(k-r+1)(k-r+2)(k-r+3)f(r)f(k-r+3)\end{array}\right) \\ -2N_2^2\sum_{r=0}^{k}((k-r+1)(k-r+2)m(r)m(k-r+2))\end{array}\right)=0, \quad (33)$$

$$(k+1)(k+2)g(k+2)-N_1\left(\begin{array}{c} 2g(k)+\sum_{r=0}^{k}\left(\begin{array}{c}(k-r+1)\delta(r)g(k-r+1)+ \\ 2(k-r+1)g(r)f(k-r+1)- \\ 2(k-r+1)f(r)g(k-r+1)\end{array}\right) \\ +2N_2N_3\sum_{r=0}^{k}\left(\begin{array}{c}(k-r+1)m(r)n(k-r+1)- \\ (k-r+1)n(r)m(k-r+1)\end{array}\right)\end{array}\right)=0, \quad (34)$$

$$(k+1)(k+2)m(k+2)-Re_m\left(m(k)+\sum_{r=0}^{k}\left(\begin{array}{c}(k-r+1)\delta(r)m(k-r+1)- \\ 2(k-r+1)f(r)m(k-r+1)+ \\ 2(k-r+1)m(r)f(k-r+1)\end{array}\right)\right)=0, \quad (35)$$

$$(k+1)(k+2)n(k+2)-Re_m\left(\begin{array}{c} 2n(k)+\sum_{r=0}^{k}\left(\begin{array}{c}(k-r+1)\delta(r)n(k-r+1)- \\ 2(k-r+1)f(r)n(k-r+1)\end{array}\right) \\ +2(N_2/N_3)\sum_{r=0}^{k}((k-r+1)m(r)g(k-r+1))\end{array}\right)=0, \quad (36)$$

where $f(k)$, $g(k)$, $m(k)$ and $n(k)$ are the differential transforms of $f(\eta)$, $g(\eta)$, $m(\eta)$ and $n(\eta)$ are displayed by:

$$f(\eta) = \sum_{k=0}^{\infty} f(k)\eta^k, \tag{37}$$

$$g(\eta) = \sum_{k=0}^{\infty} g(k)\eta^k, \tag{38}$$

$$m(\eta) = \sum_{k=0}^{\infty} m(k)\eta^k, \tag{39}$$

$$n(\eta) = \sum_{k=0}^{\infty} n(k)\eta^k, \tag{40}$$

$$\begin{aligned} &f(0) = 0,\, f(1) = 0,\, f(2) = \alpha,\, f(3) = \beta, \\ &g(0) = 1,\, g(1) = \gamma,\, m(0) = 0,\, m(1) = \kappa,\, n(0) = 0,\, n(1) = \omega, \end{aligned} \tag{41}$$

where α, β, γ, κ and ω are constants. By substituting Eq (41) into Eqs (33)–(36), we obtain the values of $f(\eta)$, $g(\eta)$, $m(\eta)$ and $n(\eta)$.

$$f(\eta) = \alpha\eta^2 + \beta\eta^3 + \frac{1}{4}N_1\alpha\eta^4 + \frac{1}{5}N_1\beta\eta^5 + \cdots, \tag{42}$$

$$\begin{aligned} g(\eta) = 1 + \gamma\eta + N_1\eta^2 + \frac{1}{6}N_1(4\alpha + 3\gamma)\eta^3 + \frac{1}{12}N_1(4N_1 + 6\beta + 2\alpha\gamma)\eta^4 \\ + \frac{1}{20}N_1\begin{pmatrix} 2N_1\alpha + 4\beta\gamma + \frac{5}{6}N_1(4\alpha + 3\gamma) + \\ 2N_2N_3\left(-\frac{2}{3}Re_m\kappa\omega + \frac{1}{3}Re_m\kappa\left(\frac{2N_2\gamma\kappa}{N_3} + 3\omega\right)\right) \end{pmatrix}\eta^5 + \cdots, \end{aligned} \tag{43}$$

$$m(\eta) = \kappa\eta + \frac{1}{3}Re_m\kappa\eta^3 + \frac{1}{6}Re_m\alpha\kappa\eta^4 + \frac{1}{20}Re_m\left(\frac{4Re_m\kappa}{3} + 4\beta\kappa\right)\eta^5 + \cdots, \tag{44}$$

$$\begin{aligned} n(\eta) = \omega\eta + \frac{1}{6}Re_m\left(\frac{2N_2\gamma\kappa}{N_3} + 3\omega\right)\eta^3 + \frac{1}{12}Re_m\left(\frac{4N_1N_2\kappa}{N_3} - 2\alpha\omega\right)\eta^4 + \\ \frac{1}{20}Re_m\left(\frac{2N_2Re_m\gamma\kappa}{3N_3} + \frac{N_1N_2(4\alpha + 3\gamma)\kappa}{N_3} - 2\beta\omega + \frac{5}{6}Re_m\left(\frac{2N_2\gamma\kappa}{N_3} + 3\omega\right)\right)\eta^5 + \cdots, \end{aligned} \tag{45}$$

where the number of required terms is determined by the convergence of the numerical values to one's desired accuracy. We obtain the approximants using *MATHEMATICA* software. The Padé approximant is employed to extend the convergence radius of the truncated series solution. As it is illustrated in Figs 2–3, without using the Padé approximant, the different orders of DTM solution cannot satisfy boundary conditions at infinity. Therefore, it is necessary to apply DTM-Padé to provide an effective way to handle infinite boundary value problems. The Padé approximant is applied to Eqs (42)–(45) and one can obtain α, β, γ, κ and ω.

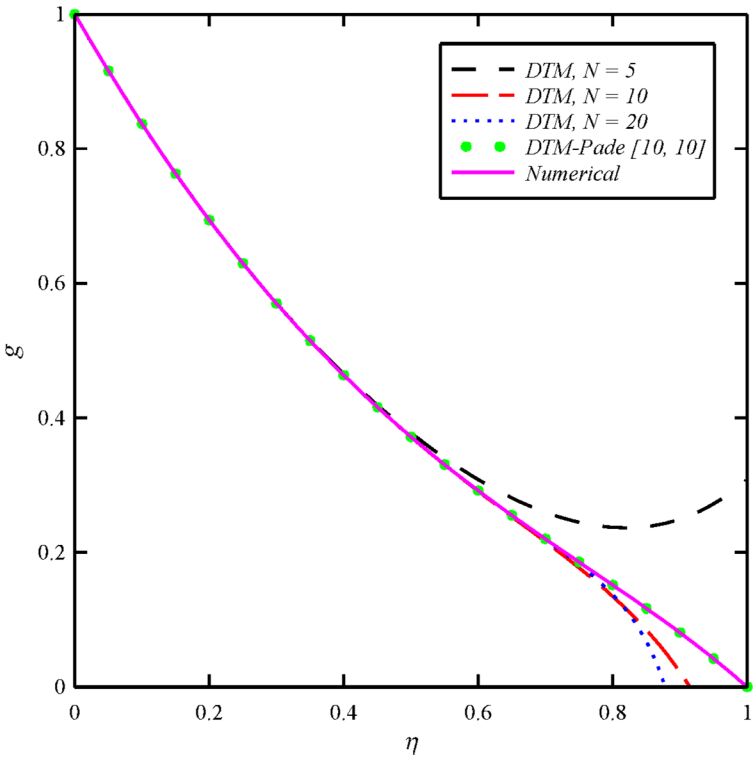

Fig 2. The obtained results of tangential velocity distribution (*g*) for different orders of DTM and DTM-Padé solutions in comparison with the numerical solution when $N_1 = N_2 = N_3 = 1$ and $Bt = 6$.

doi:10.1371/journal.pone.0135004.g002

Results and Discussion

The nonlinear ordinary differential equations subject to the boundary conditions are solved via DTM-Padé method for some values of the four key parameters i.e. squeeze Reynolds number (N_1), magnetic Reynolds number ($Re_m = N_1\, Bt$), dimensionless axial magnetic force parameter (N_2), dimensionless tangential magnetic force parameter (N_3) on the velocity and induced magnetic field components in the gap between the disks and also on the torques at the lower and upper disk. Computations are performed for the evolution of velocity components (f, g) and induced magnetic field components (m, n) with dimensionless axial coordinate (η). Representative values are used to simulate physically realistic flows. Table 1 and Table 2 present the comparison between the DTM-Padé and numerical solution, based on shooting technique, results for torque values at lower ($dg(0)/d\eta$) and upper disk ($dg(1)/d\eta$) for various values of squeeze Reynolds number (N_1) and axial magnetic force number (N_2).

Figs 4, 5, 6 and 7 display the effects of magnetic Reynolds number (Re_m) on the axial and tangential velocity distributions and induced magnetic field distributions (f, g, m, n). The magnetic Reynolds number defines the ratio of the fluid flux to the magnetic diffusivity. This parameter therefore is instrumental in determining the diffusion of magnetic field along streamlines and is analogous to the classical Reynolds number in viscous hydrodynamics, the latter controlling the vorticity diffusion along the streamlines. When N_1 is large this implies fast vertical velocity of the upper disk and vice versa for small values of this squeezing parameter. The variation in Re_m has almost little effect on the axial velocity distribution. As it is obvious from Fig 5, the maximum values of g arises at the lower disk ($\eta = 0$) for all cases. In other word, the azimuthal velocity of the fluid decreases as we move from the lower disk towards the

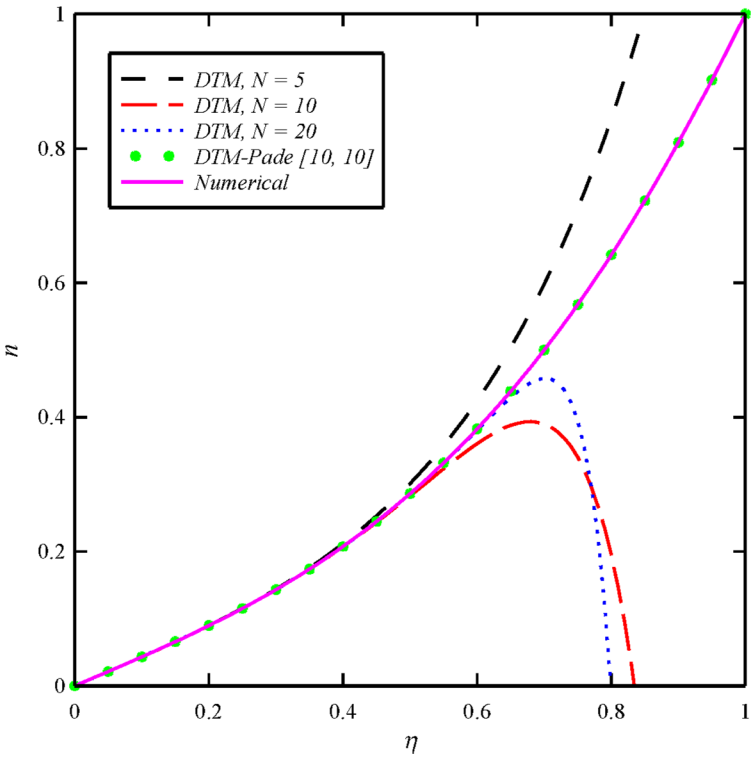

Fig 3. The obtained results of tangential induced magnetic field distribution (*n*) for different orders of DTM and DTM-Padé solutions in comparison with the numerical solution when $N_1 = N_2 = N_3 = 1$ and $Bt = 6$.

doi:10.1371/journal.pone.0135004.g003

upper disk. In addition, the tangential velocity distribution is a decreasing function of magnetic Reynolds number. With an increase in Re_m from 1, 2 through to the maximum value of 10, there is a strong decrease in the axial induced magnetic field component (m) and tangential induced magnetic field component (n). For all cases the maximum values of m and n arise at the upper disk ($\eta = 1$). It is to certify that for higher values of Re_m the squeeze film must possess much higher electrical conductivities.

The effects of dimensionless axial magnetic force parameter (N_2) on the axial and tangential velocity distributions and induced magnetic field distributions (f, g, m, n) are illustrated in Figs 8, 9, 10 and 11. Axial velocity is generated in the two-disk system from the vertical motion of the upper disk and the radial flux far from the axis of rotation in the vicinity of the lower disk. When N_2 is large this means fast vertical velocity of the upper disk and vice versa for small N_2.

Table 1. Torque values at lower ($dg(0)/d\eta$) and upper disk ($dg(1)/d\eta$) when $N_2 = 1$, $N_3 = 0.5$ and $Bt = 6$ for various N_1.

N_1	$\frac{dg(0)}{d\eta}$		$\frac{dg(1)}{d\eta}$	
	DTM-Padé Result	Numerical Result	DTM-Padé Result	Numerical Result
0.1	– 1.08963495	– 1.08963506	– 0.95987351	– 0.95987349
0.2	– 1.17203735	– 1.17203765	– 0.93844853	– 0.93844830
0.3	– 1.25013614	– 1.25013649	– 0.92615659	– 0.92615609
0.5	– 1.39797802	– 1.39797797	– 0.91295668	– 0.91295593
1	– 1.73306809	– 1.73306821	– 0.89280560	– 0.89280536
2	– 2.28925264	– 2.28925762	– 0.83902287	– 0.83902117

doi:10.1371/journal.pone.0135004.t001

Table 2. Torque values at lower ($dg(0)/d\eta$) and upper disk ($dg(1)/d\eta$) $N_1 = 1$, $N_3 = 0.5$ and $Bt = 6$ for various N_2.

N_2	$\frac{dg(0)}{d\eta}$		$\frac{dg(1)}{d\eta}$	
	DTM-Padé Result	Numerical Result	DTM-Padé Result	Numerical Result
0	– 1.77239023	– 1.77238909	– 0.60923829	– 0.60923369
1	– 1.73306809	– 1.73306821	– 0.89280560	– 0.89280536
2	– 1.62765012	– 1.62765091	– 1.91333401	– 1.91333213
3	– 1.48539942	– 1.48539918	– 3.92694971	– 3.92694747
4	– 1.34565346	– 1.34565395	– 6.89037665	– 6.89038054
5	– 1.23080507	– 1.23080496	– 10.44130841	– 10.44131517

doi:10.1371/journal.pone.0135004.t002

It can be seen that an increase in N_2 from 0 to 5 induces a significant decrease in the axial velocity between the disks. The tangential velocity distribution (g) is also directly affected by an increase in squeeze Reynolds number. As the axial component of the magnetic force N_2 increases, the azimuthal velocity g increases. Hence, the axial magnetic force N_2 can be used to increase the azimuthal velocity of the fluid. The increase of g with N_2 agrees with the results obtained by Elshekh and Elhady [24] and Hamza [43]. The effect of the magnetic force N_2 will be dominant Ω_1. As the results present, an increase in the dimensionless axial magnetic force parameter causes to decrease the axial induced magnetic field distribution (m) and increase in the tangential induced magnetic field distribution (n). The tangential velocity profile and tangential induced magnetic field also become significantly more curved with higher N_2 values. The current results are an expected result since the normal component of the induced magnetic

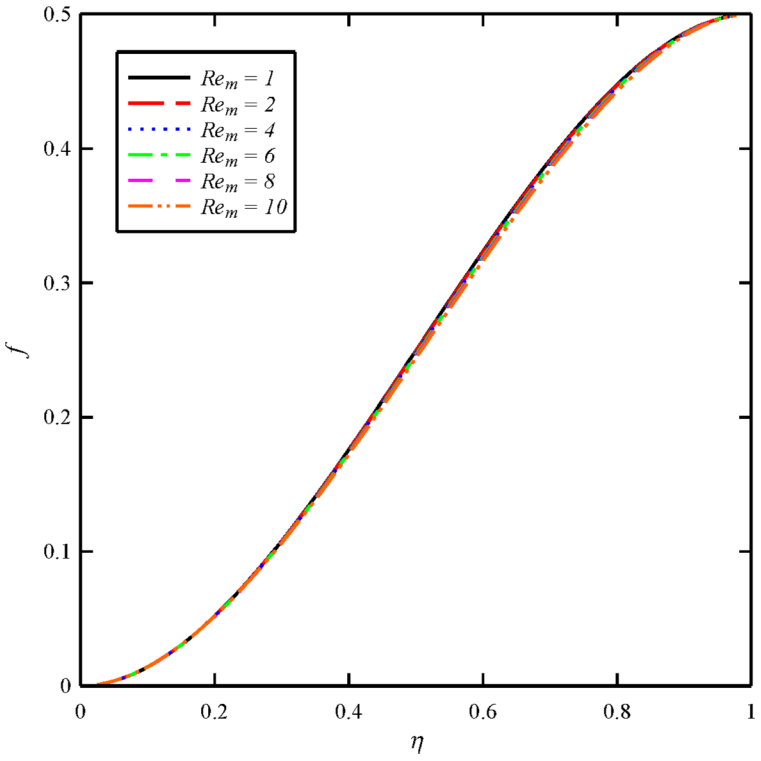

Fig 4. Effect of magnetic Reynolds number (Re_m) on the axial velocity distribution (f) when $N_2 = 1$, $N_3 = 0.5$ and $Bt = 6$.

doi:10.1371/journal.pone.0135004.g004

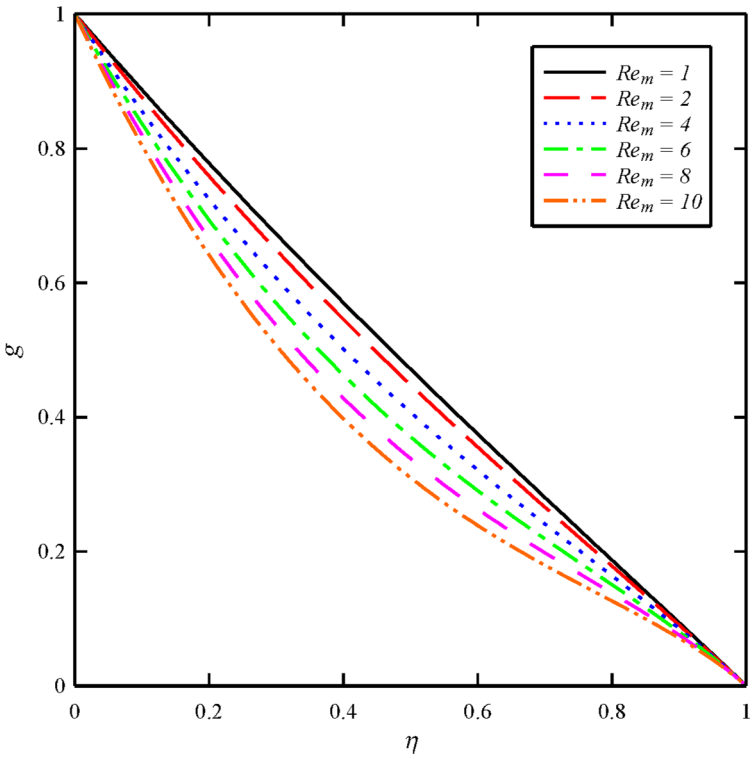

Fig 5. Effect of magnetic Reynolds number (Re_m) on the tangential velocity distribution (g) when N_2 = 1, N_3 = 0.5 and Bt = 6.

doi:10.1371/journal.pone.0135004.g005

field between the two disks must increase with the increase of the normal component of the external applied magnetic field.

Figs 12 and 13 depict the effect of dimensionless tangential magnetic force parameter (N_3) on the tangential velocity distribution (g) and tangential induced magnetic field distribution (n), respectively. The tangential velocity distribution slightly increases with the increases in the dimensionless tangential magnetic force parameter from 0.5 to 5. Increasing the dimensionless tangential magnetic force parameter causes to decreases the tangential induced magnetic field distribution.

Conclusions

The present study has displayed novel DTM-Padé solution, the combination of differential transform method and Padé approximation, for two nonlinear magneto-hydrodynamic squeeze film problems. Applications of the study include in automotive magneto-rheological shock absorbers, novel aircraft landing gear systems and biological prosthetics. The transformed dimensionless equations have been formulated and solved with robust boundary conditions. Exceptional stability and convergence characteristics have been demonstrated with the DTM. The physical key parameters emerging have been investigated graphically in detail including dimensionless axial magnetic force strength parameter, dimensionless tangential magnetic force strength parameter and magnetic Reynolds number. The results illustrated that the tangential velocity distribution is a decreasing function of magnetic Reynolds number. Further, the tangential velocity distribution is directly affected by an increase in squeeze Reynolds number. In addition, an increase in the dimensionless axial magnetic force parameter causes to decrease the axial induced magnetic field distribution and increase in the tangential induced

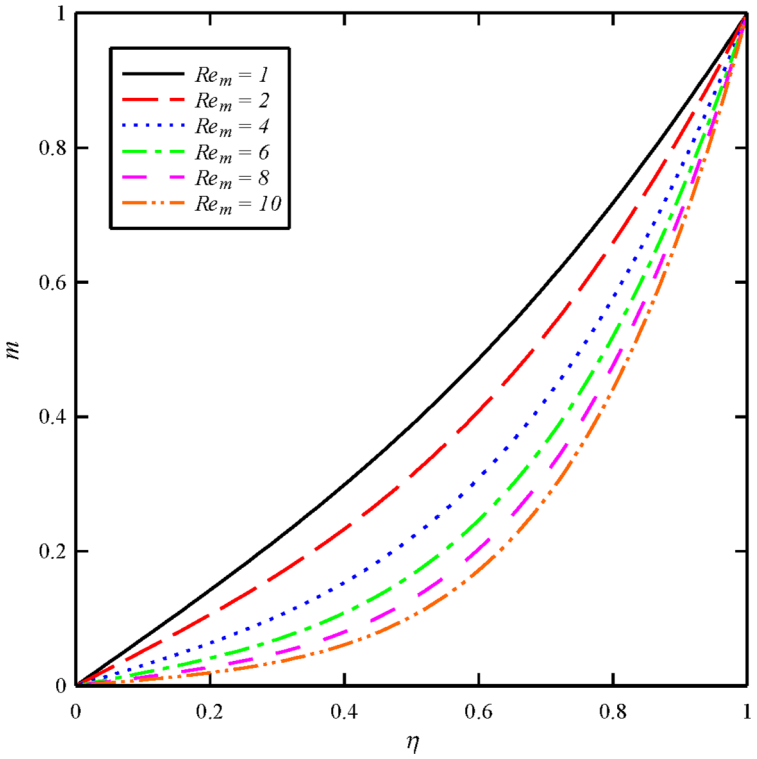

Fig 6. Effect of magnetic Reynolds number (Re_m) on the axial induced magnetic field distribution (m) when $N_2 = 1$, $N_3 = 0.5$ and $Bt = 6$.

doi:10.1371/journal.pone.0135004.g006

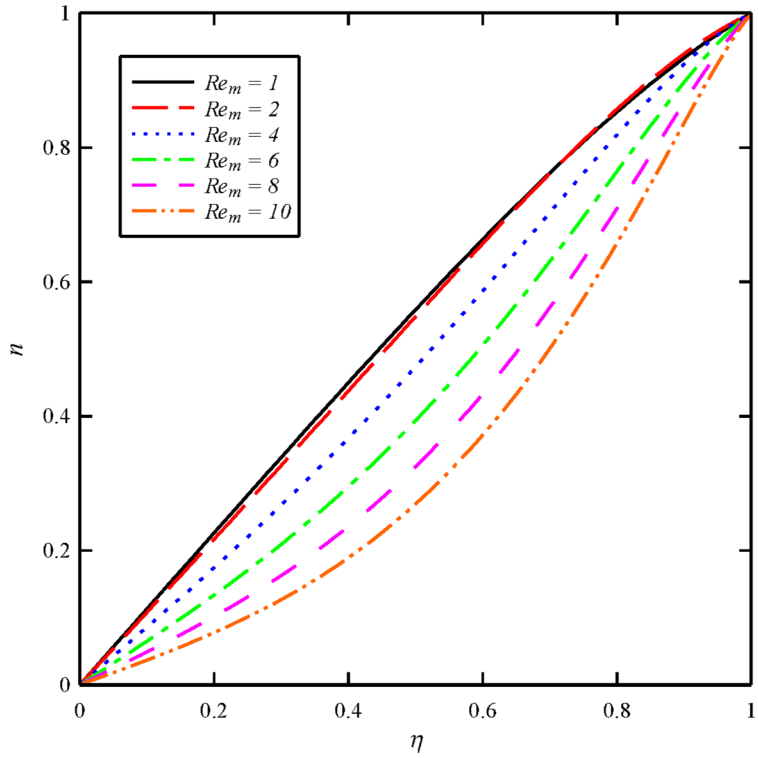

Fig 7. Effect of magnetic Reynolds number (Re_m) on the tangential induced magnetic field distribution (n) when $N_2 = 1$, $N_3 = 0.5$ and $Bt = 6$.

doi:10.1371/journal.pone.0135004.g007

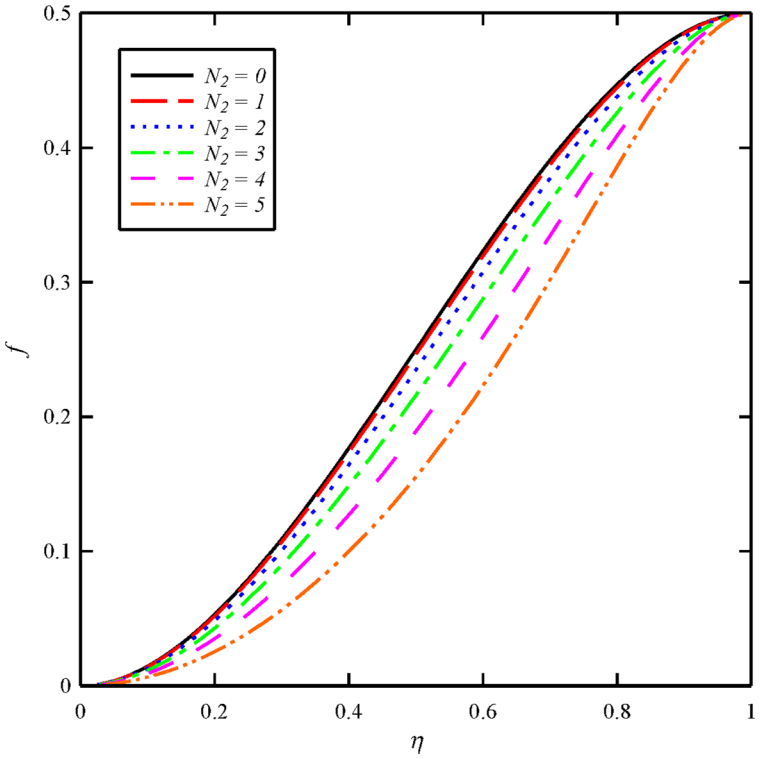

Fig 8. Effect of axial magnetic force number (N_2) on the axial velocity distribution (f) when $N_1 = 1$, $N_3 = 0.5$ and $Bt = 6$.

doi:10.1371/journal.pone.0135004.g008

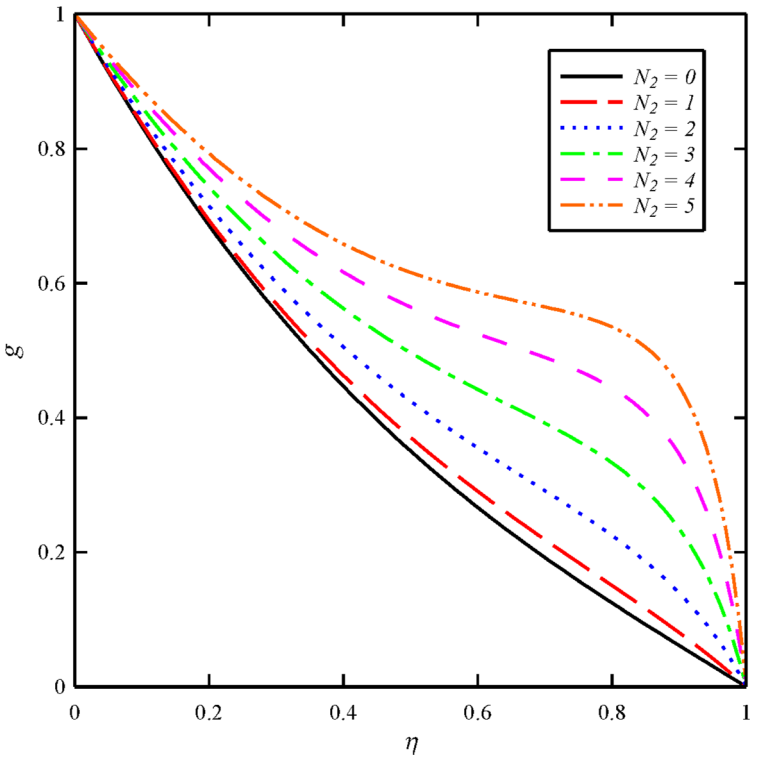

Fig 9. Effect of axial magnetic force number (N_2) on the tangential velocity distribution (g) when $N_1 = 1$, $N_3 = 0.5$ and $Bt = 6$.

doi:10.1371/journal.pone.0135004.g009

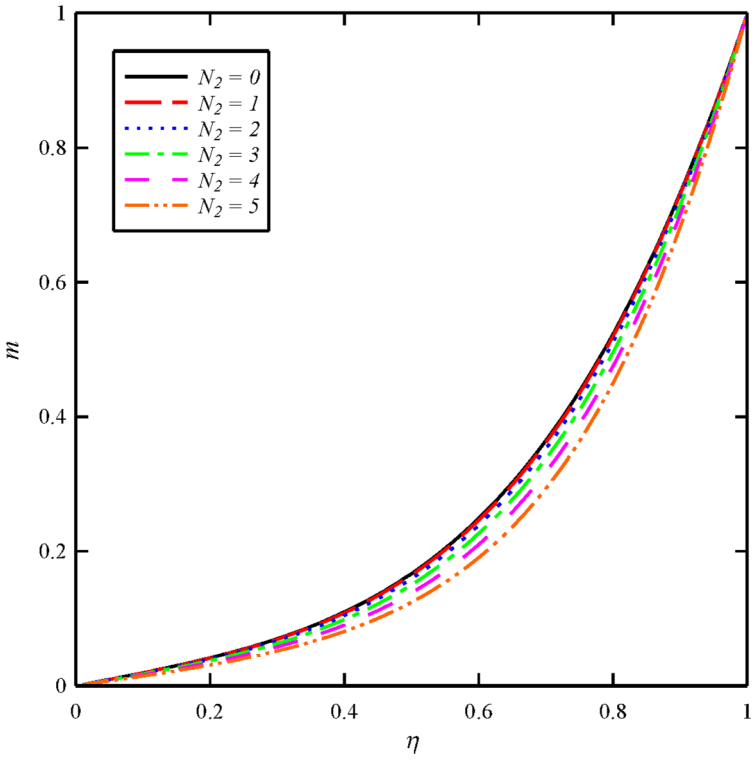

Fig 10. Effect of axial magnetic force number (N_2) on the axial induced magnetic field distribution (m) when $N_1 = 1$, $N_3 = 0.5$ and $Bt = 6$.

doi:10.1371/journal.pone.0135004.g010

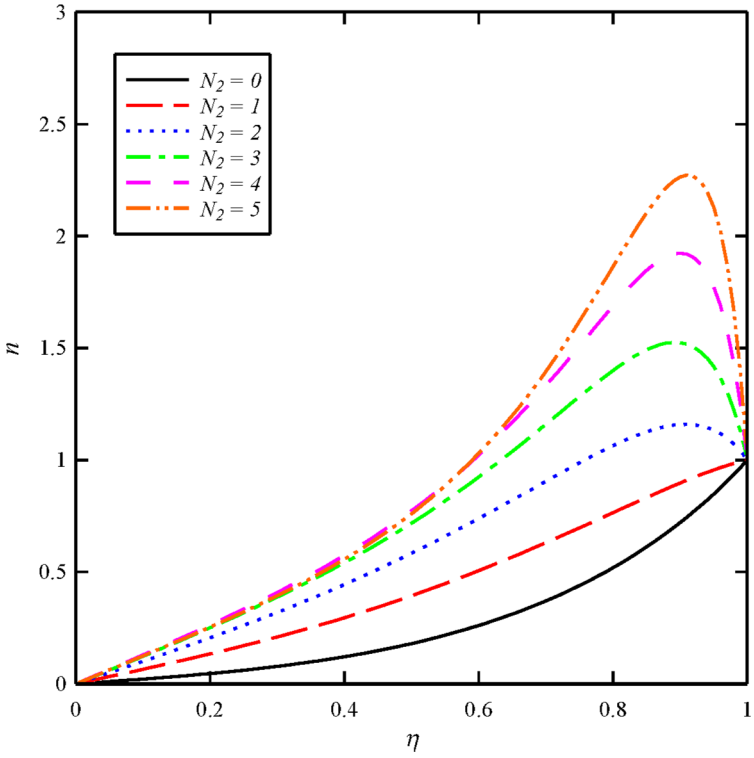

Fig 11. Effect of axial magnetic force number (N_2) on the tangential induced magnetic field distribution (n) when $N_1 = 1$, $N_3 = 0.5$ and $Bt = 6$.

doi:10.1371/journal.pone.0135004.g011

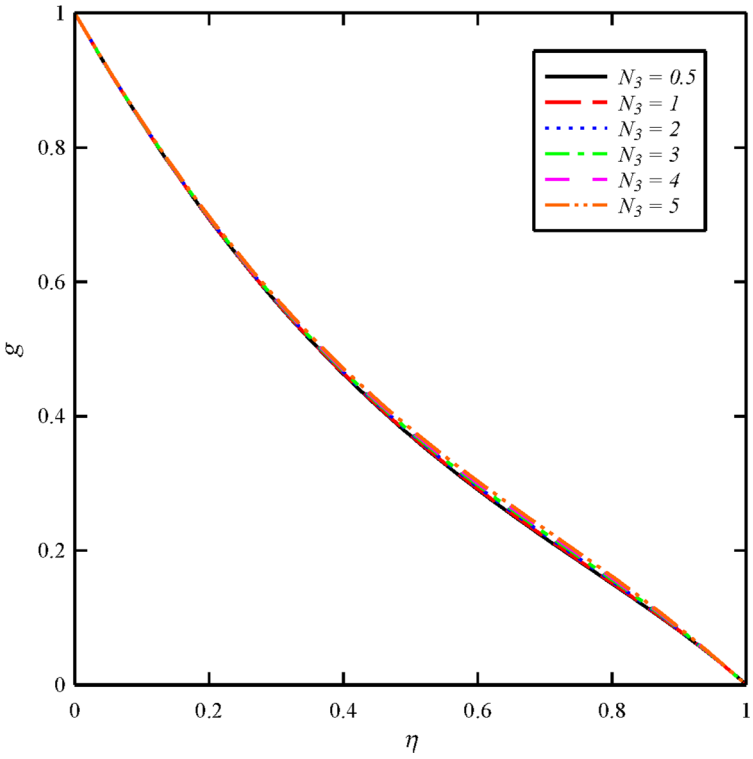

Fig 12. Effect of tangential magnetic force number (N_3) on the tangential velocity distribution (g) when $N_1 = N_2 = 1$, and $Bt = 6$.

doi:10.1371/journal.pone.0135004.g012

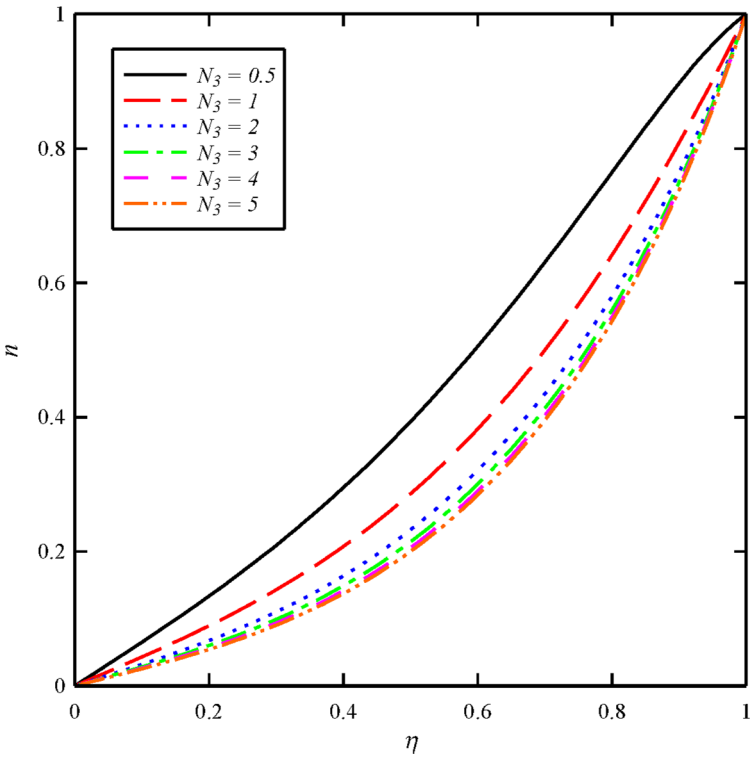

Fig 13. Effect of tangential magnetic force number (N_3) on the tangential induced magnetic field distribution (n) when $N_1 = N_2 = 1$, and $Bt = 6$.

doi:10.1371/journal.pone.0135004.g013

magnetic field distribution. Moreover, increasing the dimensionless tangential magnetic force parameter causes to decreases the tangential induced magnetic field distribution.

Acknowledgments

EM acknowledges support from the National Research foundation of South Africa.

Author Contributions

Conceived and designed the experiments: MMR NF BR. Performed the experiments: NF BR. Analyzed the data: MMR EM. Contributed reagents/materials/analysis tools: MMR NF EM BR. Wrote the paper: MMR NF EM BR.

References

1. Davidson P A. An introduction to magnetohydrodynamics. Cambridge University Press, 2001.
2. Rashidi M M, Rostami B, Freidoonimehr N, Abbasbandy S.Free convective heat and mass transfer for MHD fluid flow over a permeable vertical stretching sheet in the presence of the radiation and buoyancy effects. Ain Shams Engineering Journal 5 (2014) 901–912.
3. Khan A, Khan I, Ali F, ulhaq S, Shafie S, Effects of Wall Shear Stress on Unsteady MHD Conjugate Flow in a Porous Medium with Ramped Wall Temperature, PLOS ONE 9 (2014) e90280. doi: 10.1371/journal.pone.0090280 PMID: 24621775
4. Hussanan A, Ismail Z, Khan I, Hussein A, Shafie S, Unsteady boundary layer MHD free convection flow in a porous medium with constant mass diffusion and Newtonian heating, The European Physical Journal Plus 129 (2014) 1–16.
5. Samiulhaq, Ahmad S, Vieru D, Khan I, Shafie S, Unsteady Magnetohydrodynamic Free Convection Flow of a Second Grade Fluid in a Porous Medium with Ramped Wall Temperature, PLOS ONE 9 (2014) e88766. doi: 10.1371/journal.pone.0088766 PMID: 24785147
6. Khan A, Khan I, Ali F, Shafie S, Effects of Wall Shear Stress on MHD Conjugate Flow over an Inclined Plate in a Porous Medium with Ramped Wall Temperature, Mathematical Problems in Engineering 2014 (2014) 15 pages.
7. Khalid A, Khan I, Khan A, Shafie S, Unsteady MHD free convection flow of Casson fluid past over an oscillating vertical plate embedded in a porous medium, Engineering Science and Technology, an International Journal.
8. Park E, Min K-W, Lee S-K, Lee S-H, Lee H-J, Moon S-J, et al., Real-time hybrid test on a semi-actively controlled building structure equipped with full-scale MR dampers, Journal of Intelligent Material Systems and Structures 21 (2010) 1831–1850.
9. Anderson C G, Magnetic squeeze-films: design proposals for a magnetic-repulsion enhanced hydrostatic bearing for the type N2 wave-power buoy, Technical Report for Norwegian Institute of Technology-Trondheim, Dept. Mechanical Engineering, Edinburgh University, Scotland (1983).
10. Chernyakova Y M, Pinchuk L S, Lobanovskii L. S, Drozd E S, Chizhik S A, Structure and magnetic susceptibility of lubricating fluids in synovial joints, Journal of Friction and Wear 32 (2011) 54–60.
11. Liu B, Li W H, Kosasih P B, Zhang X Z, Development of an MR-brake-based haptic device, Smart Materials and Structures 15 (2006) 1960.
12. Chandra P, Sinha P, Kumar D, Ferrofluid lubrication of a journal bearing considering cavitation, Tribology Transactions 35 (1992) 163–169.
13. Song W L, Choi S-B, Choi J Y, Lee C H, Wear and friction characteristics of magnetorheological fluid under magnetic field activation, Tribology Transactions 54 (2011) 616–624.
14. Durán J D G, Iglesias G R, Delgado A V, Ruiz-Morón L F, Insa J, González-Caballero F, Stability and Flow Behavior of a Magnetorheological Lubricant in a Magnetic Shock Absorber, Tribology Transactions 51 (2008) 271–277.
15. Huang W, Shen C, Liao S, Wang X, Study on the Ferrofluid Lubrication with an External Magnetic Field, Tribology Letters 41 (2011) 145–151.
16. Stolarski T A, Makida Y, Performance of Lubricated Sliding Contact in Magnetic Field, Tribology Letters 46 (2012) 113–121.
17. Anwar M I, Rodkiewicz C M, Nonuniform Magnetic Field Effects in MHD Slider Bearing, Journal of Tribology 94 (1972) 101–105.

18. Kargulewicz M, Iordanoff I, Marrero V, Tichy J, Modeling of Magnetorheological Fluids by the Discrete Element Method, Journal of Tribology 134 (2012) 031706–031706.
19. Zueco J, Bég O A, Network numerical analysis of hydromagnetic squeeze film flow dynamics between two parallel rotating disks with induced magnetic field effects, Tribology International 43 (2010) 532–543.
20. Zhu G, Ingber M S, Accurate treatment of lubrication forces between rigid spheres in viscous fluids using a traction-corrected boundary element method, Engineering Analysis with Boundary Elements 33 (2009) 467–473.
21. Gertzos K P, Nikolakopoulos P G, Papadopoulos C A, CFD analysis of journal bearing hydrodynamic lubrication by Bingham lubricant, Tribology International 41 (2008) 1190–1204.
22. Asadi M, Rashidi M M, Bég T A, Bég O A, Homotopy analysis of transient magneto-bio-fluid dynamics of micropolar squeeze film in a porous medium: A model for magneto-bio-rheological lubrication. Journal of Mechanics in Medicine and Biology 12 (2012) 1250051.
23. Moghani T, Butler J P, Lin J L-W, Loring S H.Finite element simulation of elastohydrodynamic lubrication of soft biological tissues. Computers & Structures 85 (2007) 1114–1120.
24. Elshekh S S, Abd Elhady M K.Fluid film squeezed between two rotating disks in the presence of a magnetic field. International Journal of Engineering Science 34 (1996) 1183–1195.
25. Gul T, Islam S, Shah R A, Khan I, Khalid A, Shafie S. Heat Transfer Analysis of MHD Thin Film Flow of an Unsteady Second Grade Fluid Past a Vertical Oscillating Belt. PLOS ONE 9 (2014) e103843. doi: 10.1371/journal.pone.0103843 PMID: 25383797
26. Gul T, Islam S, Shah R A, Khan I, Shafie S, Khan M A. Analysis of thin film flow over a vertical oscillating belt with a second grade fluid. Engineering Science and Technology, an International Journal.
27. Fatma A.Applications of differential transform method to differential-algebraic equations. Applied Mathematics and Computation 152 (2004) 649–657.
28. Fatma A. Solutions of the system of differential equations by differential transform method. Applied Mathematics and Computation 147 (2004) 547–567.
29. Liao S. Beyond Perturbation: Introduction to the Homotopy Analysis Method. Taylor & Francis, 2003.
30. Liao S. Advances in the Homotopy Analysis Method, World Scientific Publishing Company. Shanghai Jiao Tong University, China, 2014.
31. Dehghan M, Rahmani Y, Ganji D D, Saedodin S, Valipour M S, Rashidi S,.Convection–radiation heat transfer in solar heat exchangers filled with a porous medium: Homotopy perturbation method versus numerical analysis. Renewable Energy 74 (2015) 448–455.
32. Sheikholeslami M, Ganji D D, Ashorynejad H R, Rokni H B. Analytical investigation of Jeffery-Hamel flow with high magnetic field and nanoparticle by Adomian decomposition method. Applied Mathematics and Mechanics 33 (2012) 25–36.
33. Rashidi M M, Erfani E. A new analytical study of MHD stagnation-point flow in porous media with heat transfer. Computers and Fluids 40 (2011) 172–178.
34. Hamza E A, Macdonald D A. A fluid film squeezed between two parallel plane surfaces. Journal of Fluid Mechanics 109 (1981) 147–160.
35. Ibrahim F N. Unsteady flow between two rotating discs with heat transfer. Journal of Physics D: Applied Physics 24 (1991) 1293–1299
36. Ibrahim F N. Unsteady flow between two rotating discs with heat transfer. Journal of Physics D: Applied Physics 24 (1991) 1293.
37. Hughes W F, Elco R A. Magnetohydrodynamic lubrication flow between parallel rotating disks. Journal of Fluid Mechanics 13 (1962) 21–32.
38. Baker G A.Essential of padé approximants. Academic Press, London, 1975.
39. Baker G A, Graves-Morris P R, Padé approximants: Basic theory. Addison-Wesley, 1981.
40. Rashidi M M. The modified differential transform method for solving MHD boundary-layer equations. Computer Physics Communications 180 (2009) 2210–2217.
41. Rashidi M M, Mohimanian Pour S A. A novel analytical solution of heat transfer of a micropolar fluid through a porous medium with radiation by DTM-Padé. Heat Transfer—Asian Research 39 (2010) 575–589.
42. Rashidi M M, Freidoonimehr N. Series solutions for the flow in the vicinity of the equator of an MHD boundary-layer over a porous rotating sphere with heat transfer. Thermal Science 18 (2012) S527—S537.
43. Hamza E A.The magnetohydrodynamic effects on a fluid film squeezed between two rotating surfaces. Journal of Physics D: Applied Physics 24 (1991) 547.